











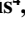
RESEARCH ARTICLE

10.1029/2021SW003016

On the Magnetosphere-Ionosphere Coupling During the May 2021 Geomagnetic Storm

Key Points:

- Global analysis of the 12 May 2021 geomagnetic storm
- Interplanetary coronal mass ejections propagation in the interplanetary space
- Magnetospheric-ionospheric coupling analysis from both particle and field point of view

M. Piersanti¹ , D. Del Moro² , A. Parmentier^{3,4}, M. Martucci^{2,4} , F. Palma^{2,4}, A. Sotgiu^{2,4}, C. Plainaki⁵ , G. D'Angelo³, F. Berrilli², D. Recchiuti^{3,6} , E. Papini³, L. Giovannelli² , G. Napolitano² , R. Iuppa^{6,7}, P. Diego³, A. Cicone¹ , M. Mergé², C. De Donato⁴ , C. De Santis⁴, R. Sparvoli^{2,4}, P. Ubertini³, R. Battiston^{6,7}, and P. Picozza^{2,4}

¹University of L'Aquila, L'Aquila, Italy, ²University of "Rome "Tor Vergata", Rome, Italy, ³National Institute of Astrophysics-IAPS, Rome, Italy, ⁴INFN - Sezione di Roma "Tor Vergata", Rome, Italy, ⁵Italian Space Agency, Rome, Italy, ⁶University of Trento, Trento, Italy, ⁷TIFPA-University of Trento, Trento, Italy

Correspondence to:

M. Piersanti,
mirko.piersanti@univaq.it

Citation:

Piersanti, M., Del Moro, D., Parmentier, A., Martucci, M., Palma, F., Sotgiu, A., et al. (2022). On the magnetosphere-ionosphere coupling during the May 2021 geomagnetic storm. *Space Weather*, 20, e2021SW003016. <https://doi.org/10.1029/2021SW003016>

Received 16 DEC 2021
Accepted 9 MAY 2022

Author Contributions:

Data curation: M. Martucci, F. Palma, A. Sotgiu, D. Recchiuti, P. Diego, M. Mergé, C. De Donato
Formal analysis: M. Piersanti, D. Del Moro, A. Parmentier, M. Martucci
Funding acquisition: P. Ubertini
Investigation: C. Plainaki, F. Berrilli
Project Administration: P. Picozza
Resources: C. De Santis
Software: M. Piersanti, D. Del Moro, G. Napolitano, A. Cicone
Supervision: P. Ubertini, R. Battiston
Validation: G. D'Angelo, C. De Donato
Visualization: F. Berrilli, D. Recchiuti, L. Giovannelli, R. Iuppa
Writing – review & editing: M. Piersanti, D. Del Moro, A. Parmentier, F. Palma, C. Plainaki, G. D'Angelo, E. Papini, A. Cicone, R. Sparvoli, P. Ubertini, R. Battiston

Abstract On 12 May 2021 the interplanetary doppelgänger of the 9 May 2021 coronal mass ejection impacted the Earth's magnetosphere, giving rise to a strong geomagnetic storm. This paper discusses the evolution of the various events linking the solar activity to the Earth's ionosphere with special focus on the effects observed in the circumterrestrial environment. We investigate the propagation of the interplanetary coronal mass ejection and its interaction with the magnetosphere—ionosphere system in terms of both magnetospheric current systems and particle redistribution, by jointly analyzing data from interplanetary, magnetospheric, and low Earth orbiting satellites. The principal magnetospheric current system activated during the different phases of the geomagnetic storm was correctly identified through the direct comparison between geosynchronous orbit observations and model predictions. From the particle point of view, we have found that the primary impact of the storm development is a net and rapid loss of relativistic electrons from the entire outer radiation belt. Our analysis shows no evidence for any short-term recovery to pre-storm levels during the days following the main phase. Storm effects also included a small Forbush decrease driven by the interplay between the interplanetary shock and subsequent magnetic cloud arrival.

Plain Language Summary On 12 May 2021 a coronal mass ejection (CME) emitted from the Sun on 9 May 2021 impacted the Earth, giving rise to a strong geomagnetic storm. This paper presents a global view of the CME effects observed in the circumterrestrial environment focusing on its propagation and on its interaction with the magnetosphere—ionosphere system in terms of both magnetospheric current systems and particle redistribution, by jointly analyzing data from interplanetary, magnetospheric, and low Earth orbiting satellites. The principal magnetospheric current system activated during the different phases of the geomagnetic storm was correctly identified through the direct comparison between geosynchronous orbit observations and model predictions. From the particle point of view, we have found that the primary impact of the storm development is a sudden loss of relativistic electrons from the entire outer radiation belt. Such kind of a global analysis is still the straightforward way available to understand the complex dynamics of the processes occurring in the circumterrestrial environment from a space weather point of view.

1. Introduction

Geomagnetic storms and substorms are among the most important signatures of the variability in the solar-terrestrial relationship. They are extremely complicated processes, which are triggered by the arrival of solar perturbations, such as interplanetary coronal mass ejections (ICMEs), solar flares, co-rotating interaction regions (CIRs), etc. (e.g., Gonzalez et al., 1994; Gosling et al., 1990; Knipp, Delores J. et al., 2021; Miyake et al., 2019; Piersanti et al., 2020). These processes, involving a wide range of plasma regions and phenomena which mutually interact with both the magnetosphere and ionosphere, are usually non linear. For the last 30 years, numerical simulations, and both ground-based and space-borne observations have been highlighting such a strong feedback and coupling process (Hayakawa et al., 2020; Navia et al., 2018; Piersanti et al., 2020; Reyes et al., 2019, and references therein). On this topic, the space weather scientific community started more and more to conduct comprehensive analysis on several "famous geomagnetic storm past events" (Boteler, 2019; Cliver Edward & Dietrich William, 2013; Hayakawa et al., 2019; Hayakawa, Hattori, et al., 2021; Knipp et al., 2018) trying to understand

© 2022. The Authors.

This is an open access article under the terms of the [Creative Commons Attribution License](https://creativecommons.org/licenses/by/4.0/), which permits use, distribution and reproduction in any medium, provided the original work is properly cited.

why extreme solar-terrestrial storms occasionally form perfect storms (Y. D. Liu et al., 2019). Those are the reasons why, in order to properly understand geomagnetic storms and substorms, it is necessary to consider the entire chain of events as a single process. When solar perturbations are analyzed, one has always to consider that the dynamic pressure of the solar wind (SW) and the interplanetary magnetic field (IMF) control the strength and the spatial structure of the magnetosphere-ionosphere current systems. The changes of these current systems are at the origin of geomagnetic activity, and consequently of the variation in the Earth's magnetospheric-ionospheric field as observed by space-borne and ground-based instruments. Indeed, a significant amount of solar wind plasma can be dropped off either directly in the polar ionosphere (polar cusp and cap) or stored into the equatorial central regions (central plasma sheet, current sheet, etc.) of the Earth's magnetospheric tail, from where it is later injected into the inner magnetospheric regions, such as the radiation belts (RBs) (Gonzalez et al., 1994), which are a pair of toroidal regions around the Earth, that are filled with magnetically-entrapped charged particles of high energy. The growth of the trapped particle population in the inner magnetosphere produces a significant increase of the ring current, while the energy released from the magnetotail and injected into the high-latitude ionosphere, together with that directly deposited in the polar regions, is responsible for an enhancement of the auroral electrojet current systems (Kivelson et al., 1995). The importance of studying these processes lies not only in the understanding of the physical processes that characterize the solar-terrestrial environment, but also in their impact on technological systems both at ground and in space, not to mention risks to human health (e.g., A. Pulkkinen et al., 2017; Baker et al., 2016; Carter et al., 2016; Dyer et al., 2018; Lanzerotti, 2001, 2017; Plainaki, Christina et al., 2020; Riley et al., 2018). Space Weather can indeed impact space-based and terrestrial technological infrastructures. Sporadic events, such as geomagnetic storms, can influence satellite and payload functions, and (in extreme cases) they can even cause the loss of a mission. In fact, a large fraction of space systems operates at altitudes of a few hundred to a few ten thousand km above the Earth's surface, in the region of the Van Allen RBs. In the Van-Allen-Probes (VAPs) Mission era, spanning the 2010s, the MagEIS and the REPT instruments on board the VAPs (Baker et al., 2013; Blake et al., 2013) returned a detailed picture of particle populations in the belts and their dynamic rearrangement triggered by solar forcing. Especially the outer radiation belt (ORB), which is dominated by energetic electrons up to several MeV, is heavily affected by geomagnetic disturbances, while the intermediate slot region, relatively devoid of electrons in quiet period due to pitch-angle scattering, can be subject to sudden refilling during strong storms (Baker et al., 2018, and references therein). On the other hand, it has been proven that the relativistic electron injection into the inner radiation belt (IRB), which is dominated by high-energy protons, is hindered by an “impenetrable barrier” at $\sim 2.8 R_E$, except for a short transient during the Halloween storm of 2003 (Baker et al., 2014).

Furthermore, it has been found that the efficiency of electron acceleration is primarily influenced by the IMF orientation and solar wind speed and dynamic pressure, and mostly achieved via resonant wave-particle interactions with VLF chorus waves (Koskinen et al., 2017; W. Li et al., 2014).

In this paper, we offer a global analysis of the 12 May 2021 geomagnetic storm, which represents a great space weather event occurring a few years after a new solar cycle onsets. We want to highlight here that despite statistical studies showed that strong geomagnetic storms take place around the maximum and in the declining phase of solar cycles (Meng et al., 2019, and reference therein), even under quiet Sun conditions significant space weather events can occur (Garcia & Dryer, 1987; Hayakawa et al., 2020; Hayakawa, Schlegel, et al., 2021; Willis & Stephenson, 2000). So the 12 May 2021 represents a significant case whose global analysis could help the current understanding about the direct link between solar driver and the relative geomagnetic response.

The paper is organized as it follows: Section 2 presents the analysis of the CME propagation in the interplanetary space; Section 3 shows the magnetosphere-ionosphere analysis; Section 4 includes the discussion and conclusions.

2. CME-Interplanetary Propagation

The solar event associated with the disturbance under analysis occurred on 9 May 2021. The source was a CME with an apparent width of $\sim 55^\circ$, which was well imaged by SOHO LASCO (Brueckner et al., 1995; Domingo et al., 1995), as well as STEREO-A COR2 (Howard et al., 2008; Kaiser et al., 2008) and HI-1 (Eyles et al., 2009).

While propagating, the ICME created an interplanetary shock that, at L1, anticipated the magnetic cloud by a few hours.

2.1. CME Lift-Off and Interplanetary Response

The CME was visually identified as a diffuse plasma structure both on STEREO-A SECCHI-COR2 and SOHO LASCO C2 FoVx (Field of Views). It enters COR2 FoV on 9 May 2021 at 11:40 UT ± 30 min and reaches the FoV edge on 9 May 2021 at 15:40 UT ± 30 min, with an estimate PoS (Plane of Sky) velocity $V_{PoS} = 600 \pm 100$ km/s. It enters LASCO C2 FoV on 9 May 2021 at 14:30 UT ± 30 min and reaches the FoV edge on 9 May 2021 at 16:00 UT ± 1 hr, with an estimate PoS velocity $V_{PoS} = 550 \pm 100$ km/s. The angle subtended by the Earth, Sun, and Stereo-A on that day was very close to 45° (see Figure 2), and subsequent observations by HI-1, which imaged the CME at a larger distance from the Sun allowed us to obtain another estimate of the ICME PoS velocity: The ICME crossed HI-1 FoV from the early hours of 10 May 2021 to late 11 May 2021 with an estimate PoS velocity of 500 km/s, obtained via the time-elongation fitting method (Barnes et al., 2019).

The most probable source for the CME was a filament eruption observed on 9 May 2021 at $t_0 = 11:30$ UT in the southern solar hemisphere (white cross in Figure 1). The filament ejection has been recorded by SDO AIA (Lemen et al., 2012; Pesnell et al., 2011) imagers. At the time of the CME lift-off, a large coronal hole (CH—Gray line in Figure 1) was present in close proximity of the filament coordinates. The CH was likely associated to a fast solar wind stream affecting the CME propagation. Considering the source on the Sun and the hypothesis of radial propagation, we can de-project the CME PoS velocities and estimate its radial velocity as $V_{rad} = 720 \pm 100$ km/s. Also, hypothesizing a cone shape for the CME and a self-similar expansion, the width of the CME can be estimated to be $50^\circ \pm 5^\circ$.

To describe the ICME propagation in the heliosphere we have used the P-DBM (Del Moro et al., 2019; Napoletano et al., 2018) model. This model assumes that the ICME dynamics is governed only by its interaction with the ambient SW. By employing a fluid dynamic analogy, the force acting on the ICME depends on the square of the ICME velocity relative to the ambient SW flow, such that the equation for the ICME radial acceleration reads:

$$a = -\gamma(r) [v - w(r)] |v - w(r)| \quad (1)$$

where $\gamma(r)$ is the so-called drag parameter representing the interaction efficiency between the ICME and the SW, $w(r)$ is the SW speed, v is the ICME speed, and r is the distance from the Sun. A good approximation beyond 20 solar radii is obtained assuming that γ and w are constant throughout the whole ICME propagation (Cargill, 2004; Vršnak et al., 2013). Under such assumptions, Equation 1 can be solved analytically providing the temporal evolution of the ICME's heliospheric distance and velocity. The P-DBM model includes in this framework the uncertainties on the initial ICME parameters and on the actual γ and w values, by means of a Probability Distribution Function and a Monte-Carlo like approach (see a detailed description in Napoletano et al., 2018, 2021). Our conjecture is that the part of the ICME hitting the Earth interacted with the fast SW generated by the CH over the whole duration of its travel, and, consequently, we have estimated its time to travel to 1AU and its velocity at arrival. From 10,000 runs of the P-DBM model, the obtained ICME's arrival time and velocity at 1AU are: $t_{1AU} = 2021-05-12 04:00 \pm 6$ h and $V_{1AU} = 640 \pm 70$ km/s. As evident from the propagation scheme reported in Figure 2, the ICME did not hit any relevant interplanetary spacecraft, nor any inner other Solar System planet.

Figure 3 shows the passage of the ICME as observed by the Wind (Lepping et al., 1995) spacecraft located at the first Lagrangian point. On 12 May 2021 at $\sim 05:55$ UT, the spacecraft detected a clear interplanetary shock (IPs—Red dashed line on the left panels), characterized by a large increase in the SW density ($\Delta n_{p,w} \approx 38$ cm $^{-3}$, panel a), velocity ($\Delta v_{sw,w} \approx 120$ km/s, panel b) and dynamic pressure ($\Delta P_{sw,w} \approx 11$ nPa, panel c), as well as in the IMF strength ($\Delta B_{IMF,w} \approx 8$ nT, panel d). Using the Rankine-Hugoniot conditions, under the assumption that both energy and momentum are conserved across the shock front (Landau et al., 1960; Oliveira, 2017), we have estimated the shock normal, obtaining the following orientation: $\Theta_{SE,W} = 177^\circ \pm 5^\circ$ and $\Phi_{SE,W} = 111^\circ \pm 5^\circ$ ($\Theta_{SE,W}$ and $\Phi_{SE,W}$ being the angles formed by the shock normal with the Sun-Earth line and with the y axis in the yz plane, respectively (Xu et al., 2020)). In addition, we have estimated the shock speed as $v_{sh,w} = 538$ km/s ± 10 km/s. The propagation of the IPs plane from WIND to the Earth's magnetopause is represented in Figure 3h using red dotted lines. From such results, under the assumption of planar propagation along the direction marked by the black arrow in Figure 3h, we have predicted both the time and location of the IPs impact onto the magne-

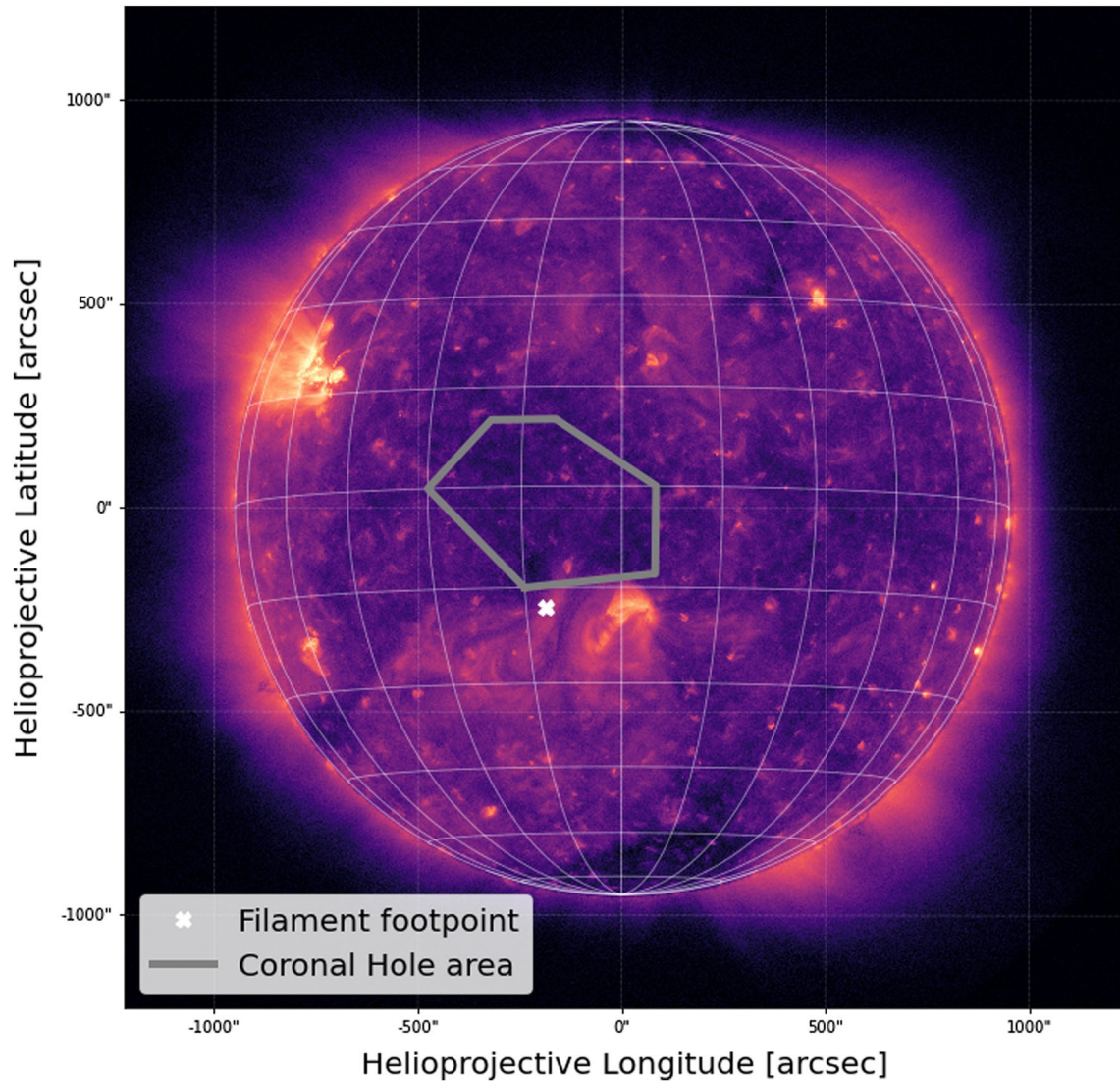


Figure 1. EUV image of the Sun by solar dynamics observatory AIA211 at the time of the filament eruption. The white cross marks the position of the filament eruption associated with the coronal mass ejection; the gray line marks the position of the coronal hole.

tosphere (green rectangle in Figure 3h), obtaining 06:34 UT (i.e., 37 min after WIND observations) and 12:49 ($\pm 00:15$) LT (i.e., in the noon sector of the magnetosphere), respectively.

The 12 May 2021 ICME was characterized by a significant magnetic cloud observed between $\sim 07:36$ UT and $\sim 15:24$ UT. Its boundaries have been determined according to the the magnetic field behavior together with temperature, velocity and density of solar protons (Burlaga et al., 1981), as depicted in the blue shaded region of Figure 3 (left panel). Indeed, plasma temperature decreases from $\sim 1.7 \cdot 10^5$ K to $\sim 6 \cdot 10^4$ K (not shown), SW speed remains almost constant at ~ 480 km/s for about 8 hr (panel b), and the total magnetic field increases to 22 nT (panel d) with a smooth, pronounced and prolonged (approximately 4 hr) southward rotation at $\approx 11:30$ UT (panel g).

The storm's main phase was followed by short-lasting substorm activity, as highlighted by |AL|-index values which dropped back to < 300 nT just after 6 hr from the occurrence of Dst minimum. This activity is likely triggered by suitable IMF preconditions (Tsurutani & Zhou, 2003), consisting in ~ 3 hr of steadily southward vertical field component upstream of the IPs.

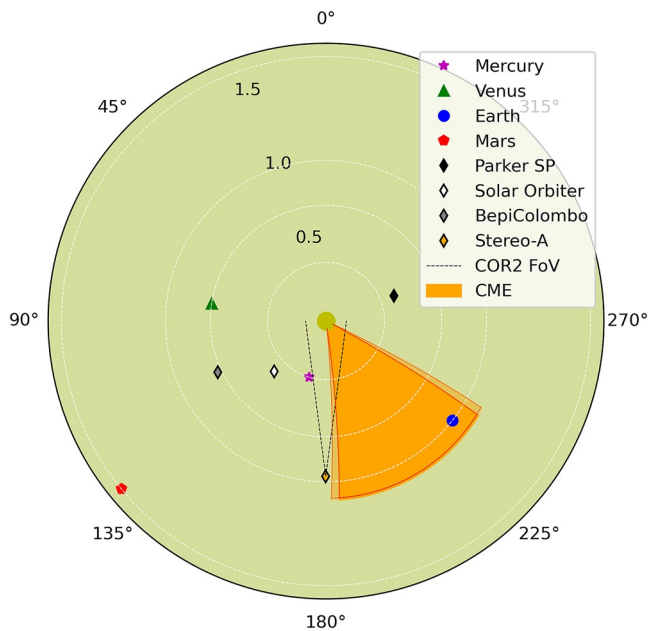


Figure 2. Geometrical properties for the propagation of the coronal mass ejection (CME) in the inner heliosphere. The positions of the inner planets and relevant spacecrafts are represented by colored symbols. The interplanetary coronal mass ejection (ICME) is represented by the orange shadowed area. The lighter orange area represent the 1σ uncertainty about the ICME position from the P-DBM runs.

3. Magnetospheric-Ionospheric Analysis

This section is dedicated to the investigation of the magnetospheric-ionospheric system during the 12 May 2021 geomagnetic storm. An accurate knowledge of the magnetosphere-ionosphere coupling dynamics, in terms of magnetospheric-ionospheric current systems and particle distribution function (A. Lui et al., 2000; Consolini & De Michelis, 2005; Milan et al., 2017; Sitnov et al., 2001), in response to the variations of the SW conditions (magnetic field orientation, plasma density, velocity, etc.) is crucial in many sectors of space weather.

3.1. Magnetosphere

Figure 4a shows the response of the magnetosphere to the arrival of the interplanetary shock. According to the Shue et al. (1998) model, the magnetopause nose moved back to $\sim 6.8R_E$. Indeed, the shapes of the magnetospheric field lines before (black lines) and soon after (red lines) the IPs, evaluated by means of the TS04 model (Tsyganenko & Sitnov, 2005), show a large field compression. Correspondingly, on May 12 at $\sim 6:35$ UT, GOES 16 (Figure 4b, left column; $LT_{G16} = UT - 5$) and GOES 17 (Figure 4b, right column; $LT_{G17} = UT - 9.1$) measured a sudden variation ($\Delta t \sim 10$ min) in the north-south component of the magnetic field ($\Delta B_{z,G16} = -28$ nT and $\Delta B_{z,G17} = 18.8$ nT), due to the compression of the magnetosphere, coupled with a stretching of the magnetotail field lines ($\Delta B_{x,G16} = 22$ nT and $\Delta B_{x,G17} = 14.6$ nT), caused by the concurring contribution of the IPs impinging onto the magnetopause and of the southward switching of the IMF (Piersanti et al., 2020; Piersanti & Villante, 2016; Villante & Piersanti, 2011).

A different situation is visible between May 12 at $\sim 11:36$ UT and May 12 at $\sim 15:24$ UT, corresponding to the arrival of the magnetic cloud. During such time interval, GOES 16 and GOES 17 were located at $06:36 < LT_{G16} < 10:24$ and $02:36 < LT_{G17} < 06:24$, respectively. In the morning side, GOES 16 observed a huge double peaks decrease along all the magnetic field components (Figure 4b, left panels). In the nightside, GOES 17 showed positive variations in both B_x and B_y components (Figure 4b, top and mid right panels), and large double peak increase along B_z (Figure 4, bottom right panel). This behavior is the signature of a strong stretching and twisting of the magnetospheric field lines and can be interpreted in terms of the concurring contribution of the partial ring current intensification and of a magnetotail current reshaping (Kalegaev et al., 2005; Ohtani et al., 2007; Piersanti et al., 2020; T. I. Pulkkinen et al., 2006). Such a scenario is confirmed by the direct comparison between a modified TS04 model (hereafter TS04*) marked by red dashed lines in Figure 4, in which we considered the contribution of the ring current and tail current (hereafter, TC) alone during the geomagnetic storm. It can be easily seen that the TS04* trace gives a good representation of the behavior of the GOES observations, confirming the key role of the ring current in the morning sector of the magnetosphere and of the tail current in the nightside sector of the magnetosphere (e.g., Kalegaev et al., 2005; Ohtani et al., 2007, and reference therein). We need to underline here that in order to have the best model representation of the magnetospheric field observations, the principal parameters of the TC in the TS04 model was customized in the following way: the hinging point R_H (defining the position of the plasma sheet bending, separating the rigidly tied near-Earth part from the more distant tailward plasma sheet) has been shifted from $8.75R_E$ to $6.85R_E$ (Dayeh et al., 2015; Tsyganenko & Sitnov, 2005; Xiao et al., 2016); the current sheet thickness D_H has been changed from $5R_E$ to $5.9R_E$ (Kan, 1973; Thompson et al., 2005; Tsyganenko & Sitnov, 2005). From a pure physical point of view, the passage of the magnetic cloud caused both a magnetospheric dipolarization and an intensification of the plasma density in the magnetotail neutral sheet, leading to a change in R_H and an increase of D_H , respectively (A. T. Y. Lui, 2016; Murphy et al., 2022, and reference therein).

The largest discrepancies between GOES measurements and TS04* predictions occurred at the peak of the main phase. Such discordance might be related to the fact that the Tsyganenko & Sitnov (2005) model estimated, at the

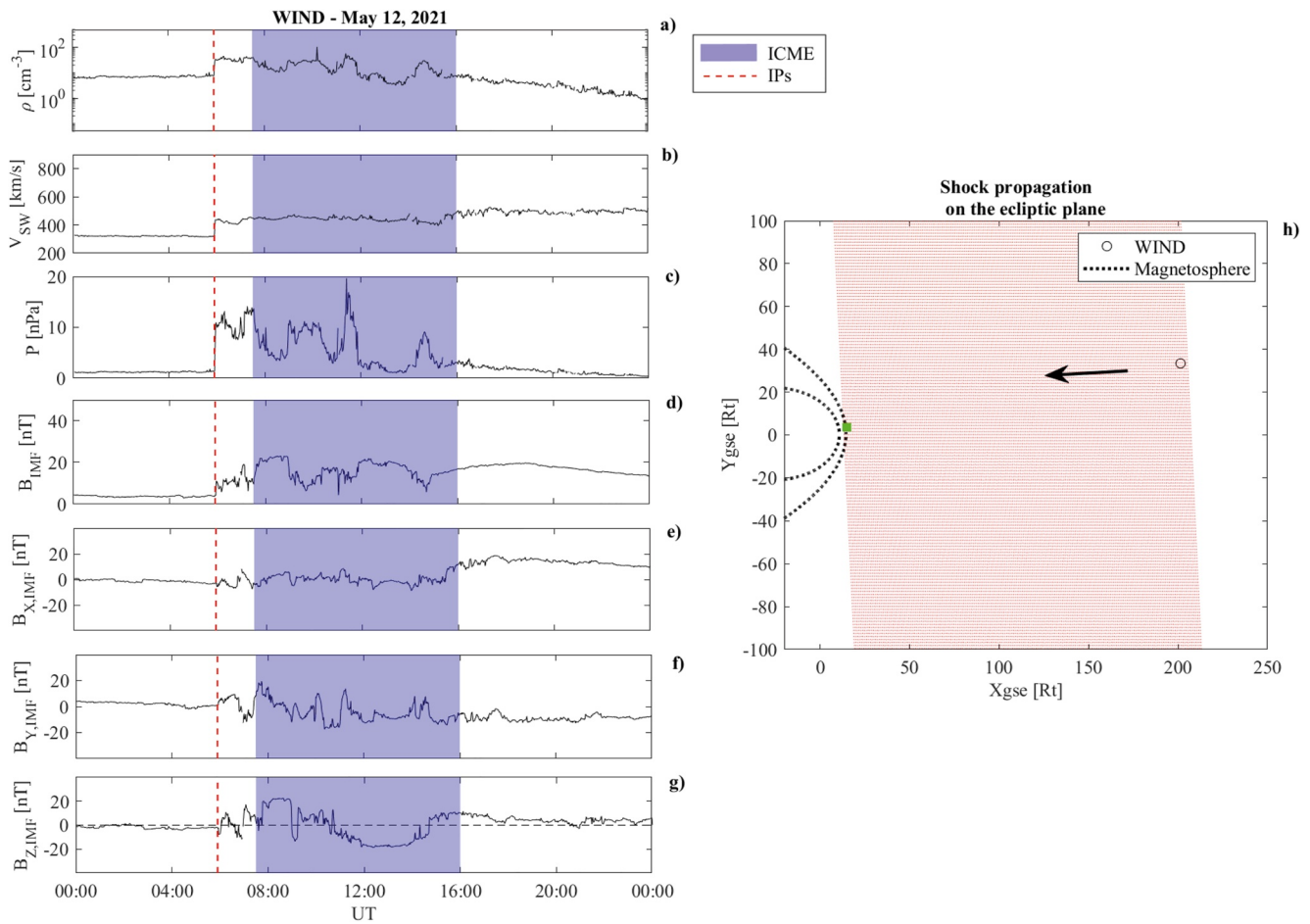


Figure 3. Solar wind parameters observed by the WIND spacecraft at L1: (a) Proton density; (b) velocity; (c) dynamic pressure; (d) interplanetary magnetic field (IMF) intensity; (e–g) IMF components ($B_{X,IMF}$, $B_{Y,IMF}$, $B_{Z,IMF}$ respectively) in the GSE reference frame. The red dashed line marks the interplanetary shock as observed on 12 May at $\approx 5:56$ UT. The blue shaded region identifies the magnetic cloud; (h) Interplanetary shock propagation in the ecliptic plane. Here red dotted lines represent the shock plane propagation in the ecliptic plane and the arrow its direction. The green rectangle represents the estimated impact position of the IPs onto the magnetopause.

peak of the main phase, a backward motion of the magnetopause up to $6.2R_E$, which is behind the GOES satellite orbit.

3.2. Ionosphere

Figure 5a shows CSES (China Seismo Electromagnetic Satellite) (Shen et al., 2018) magnetic observations (Zhou et al., 2019) along the North-South (B_N - left panel), East-West (B_E —Central panel) and Vertical (B_C —Right panel) direction, respectively, from 11 May to 14 May 2021, after removing the internal and crustal contributions to the Earth's magnetic field by use of the CHAOS-7 model (Finlay et al., 2020). CSES is a Chinese satellite launched on 2 February 2018, hosting a fluxgate magnetometer, two Langmuir probes, an electric field detector and two particle detectors out of eight payloads. The satellite orbits at about 500 km of altitude (Low Earth Orbit - LEO) in a quasi-polar Sun-synchronous orbit, and it passes at about 02:00 and 14:00 local time (LT) in its ascending and descending orbits, respectively (Shen et al., 2018).

As expected (Villante & Piersanti, 2011), the action of both the magnetospheric and ionospheric currents produced largest variations along $B_{N,Magn}$ and $B_{E,iono}$, respectively.

In order to quantify the contributions of magnetospheric and ionospheric origin at CSES orbit, we have applied the MA.I.G.I.C. model (Piersanti et al., 2019) to discriminate between different time scales in a time series. Results are shown in Figure 5b. Upper and lower panels report observations of high ($\sim 22.3 \mu\text{Hz} < f < \sim 2.8 \text{ mHz}$; f being the

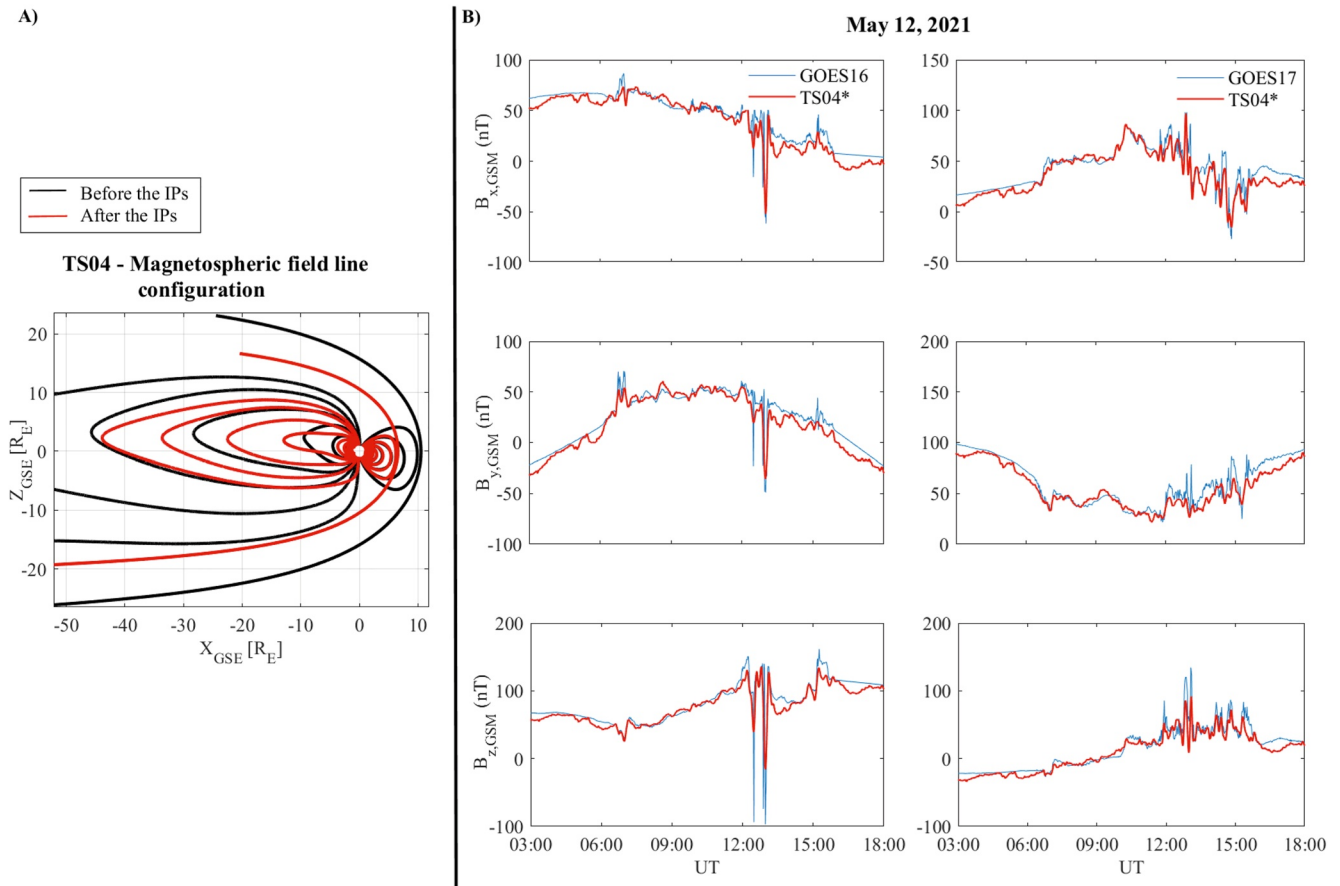


Figure 4. (a) TS04* model prediction of the magnetospheric field lines configurations before (black lines) and after (red lines) the passage of the interplanetary shock; (b): Magnetospheric field observations along X_{GSM} (upper panels), Y_{GSM} (middle panels) and Z_{GSM} (lower panels) at GOES 16 (LT = UT-5) and GOES 17 (LT = UT-9) geosynchronous orbit; red dashed lines represent the TS04*+IGRF model predictions.

frequency) and low frequency ($\sim 2.6 \mu\text{Hz} < f < \sim 21 \mu\text{Hz}$) components, respectively. The low frequency behavior shows a strong and rapid decrease along the North-South direction during the main phase of the geomagnetic storm, and a long lasting increase during the recovery phase. On the other hand, $B_{E,LF}$ and $B_{C,LF}$ show a negligible/null variation over the entire period under analysis. This behavior is consistent with field variations of magnetospheric origin induced by the action of both the asymmetric part of the ring current and tail current along $B_{N,LF}$ (Lühr & Zhou, 2020; Neubert et al., 2001; Park et al., 2020). This scenario is confirmed by the comparison between the CSES contribution of magnetospheric origin and TS04* model (red lines in Figure 5, bottom row). It can be easily seen that the TS04* model well represents the variations along $B_{N,LF}$, $B_{E,LF}$ and $B_{C,LF}$.

The high frequency components, instead, show large variations along $B_{E,HF}$. This behavior is consistent with contributions due to both the variations in the ionospheric-current system and magnetospheric-ionospheric coupling processes (e.g., field aligned current contribution). Indeed, the positive then negative variations observed in the horizontal plane during the main phase can be ascribed to the loading-unloading process between the magnetosphere and ionosphere (Consolini & De Michelis, 2005; Piersanti et al., 2020), while, the huge positive variations observed during the recovery phase can be due to the ionospheric DP-2 current system (Kamide, 1988; Kamide et al., 1997; Piersanti & Villante, 2016; Villante & Piersanti, 2011).

In order to evaluate the rearrangement of electron populations in the Earth's magnetosphere, we have applied an approach analogous to the one reported in Palma et al. (2021) for the 26 August 2018 geomagnetic storm, using particle data from the MEPED-90° electron telescope on board the NOAA19-POES satellite (Evans & Greer, 2004) and the High-Energy Particle Detector (HEPD-01) on board the CSES satellite (Picozza et al., 2019). The NOAA19-POES is Sun-synchronous nearly-polar satellite orbiting at LEO altitudes. NOAA19 is currently orbiting at an altitude of ~ 850 km with a 98.7° inclination and an orbital period of ~ 102 min. In both cases, to

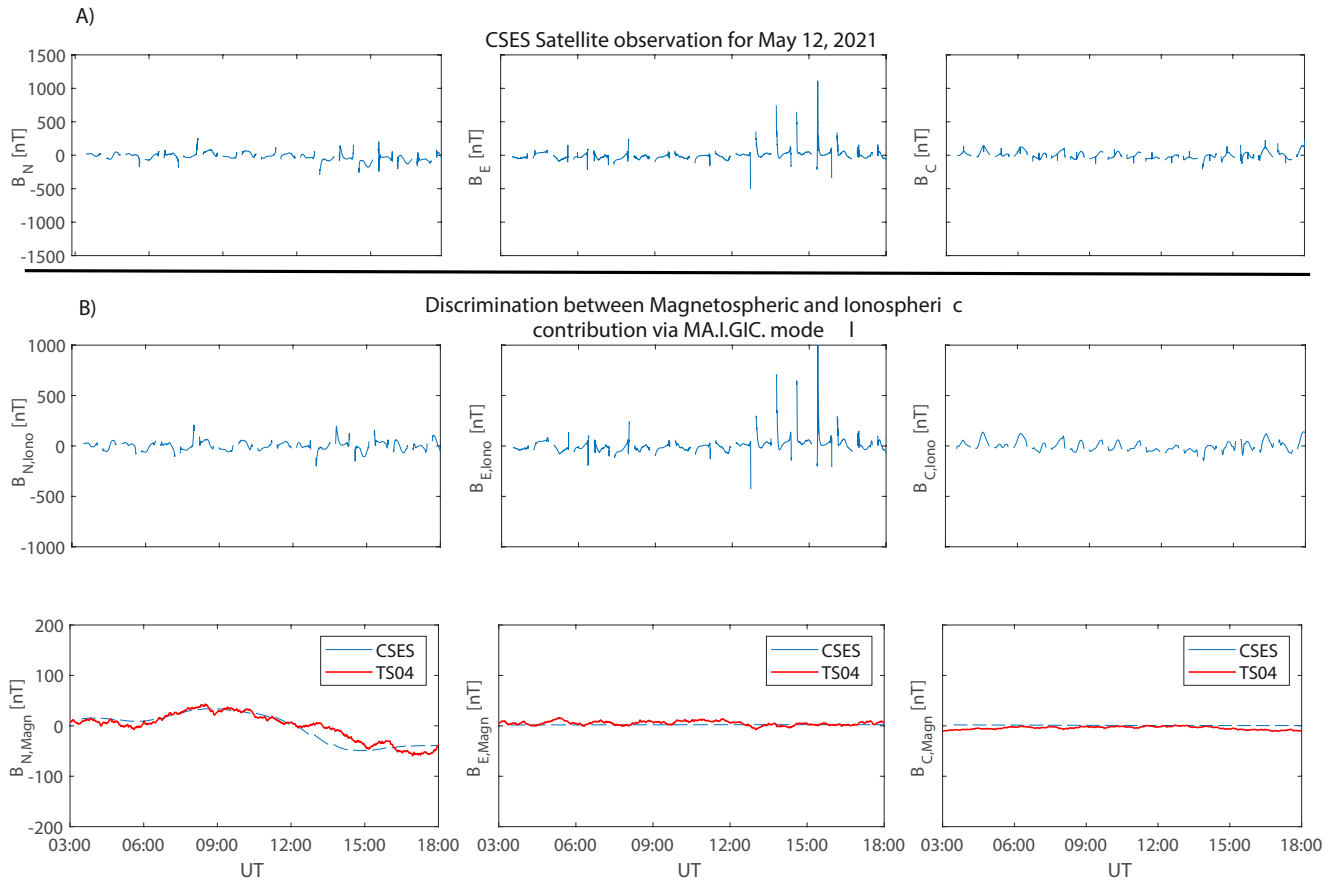


Figure 5. (a) HPM observations, for 12 May 2021, at Low Earth Orbit along geographic North-South (left panel), East-West (middle panel) and vertical (right panel) components; (b) Application of the MA.I.G.I.C. model to HPM data: Top panels show the contribution of ionospheric origin ($\sim 22.3 \mu\text{Hz} < f < \sim 2.8 \text{ mHz}$; f being the frequency time scale) for the three components of the observed field; lower panels show the contribution of magnetospheric origin ($\sim 2.6 \mu\text{Hz} < f < \sim 21 \mu\text{Hz}$) for the three components of the observed field. Red lines represent the TS04* model previsions.

avoid saturation or pile-up issues possibly occurring at extremely high particle rates, the South Atlantic Anomaly has been excluded by means of a cut in the available geomagnetic-field values (no B -values lower than 23,000 nT).

Figure 6b) depicts the behavior of MEPED integral electron fluxes over the $>0.13 \text{ MeV}$ range as a function of the McIlwain L parameter (McIlwain, 1961) throughout the pre-storm, storm, and recovery phases. The flux values, which are dominated by the contribution of low-energy electrons (Turner et al., 2015), point out a prolonged slot-filling event immediately downstream of maximum geomagnetic disturbance, characterized by flux enhancements by a few orders of magnitude. Correspondingly, the plasmapause (full black line), estimated from the X. Liu and Liu (2014) model, steps back to $L \sim 3.8$.

It is worth noticing that measurements taken in the Van-Allen-Probes era on the occasion of multiple CME-driven storms associated with IP shock compressions (Khoo et al., 2018) have established a spatial and temporal correlation between plasmapause location and the initial enhancement of energetic electrons over an energy range pretty close to the one spanned by the MEPED electron telescope in Figure 6b). At the onset of 12 May 2021 storm, the concurrent substorm activity may represent a suitable candidate for the injection of such source/seed populations to be resonantly accelerated by ULF waves at the boundary of the plasmasphere, where the plasma density gradient affects wave growth (W. Liu & Cao, 2014) and interactions.

Panels (c and d) in Figure 6 contain MEPED fluxes over the $>0.65 \text{ MeV}$ range and the rate of $>4.5 \text{ MeV}$ particles detected by HEPD-01, respectively. At L shells typical of the ORB, a persistent depletion starts right after the onset of the main phase, with no short-term flux recovery to pre-storm levels (Palma et al., 2021, and reference therein). These ORB losses in the relativistic range may be consistent with magnetopause shadowing (Herrera

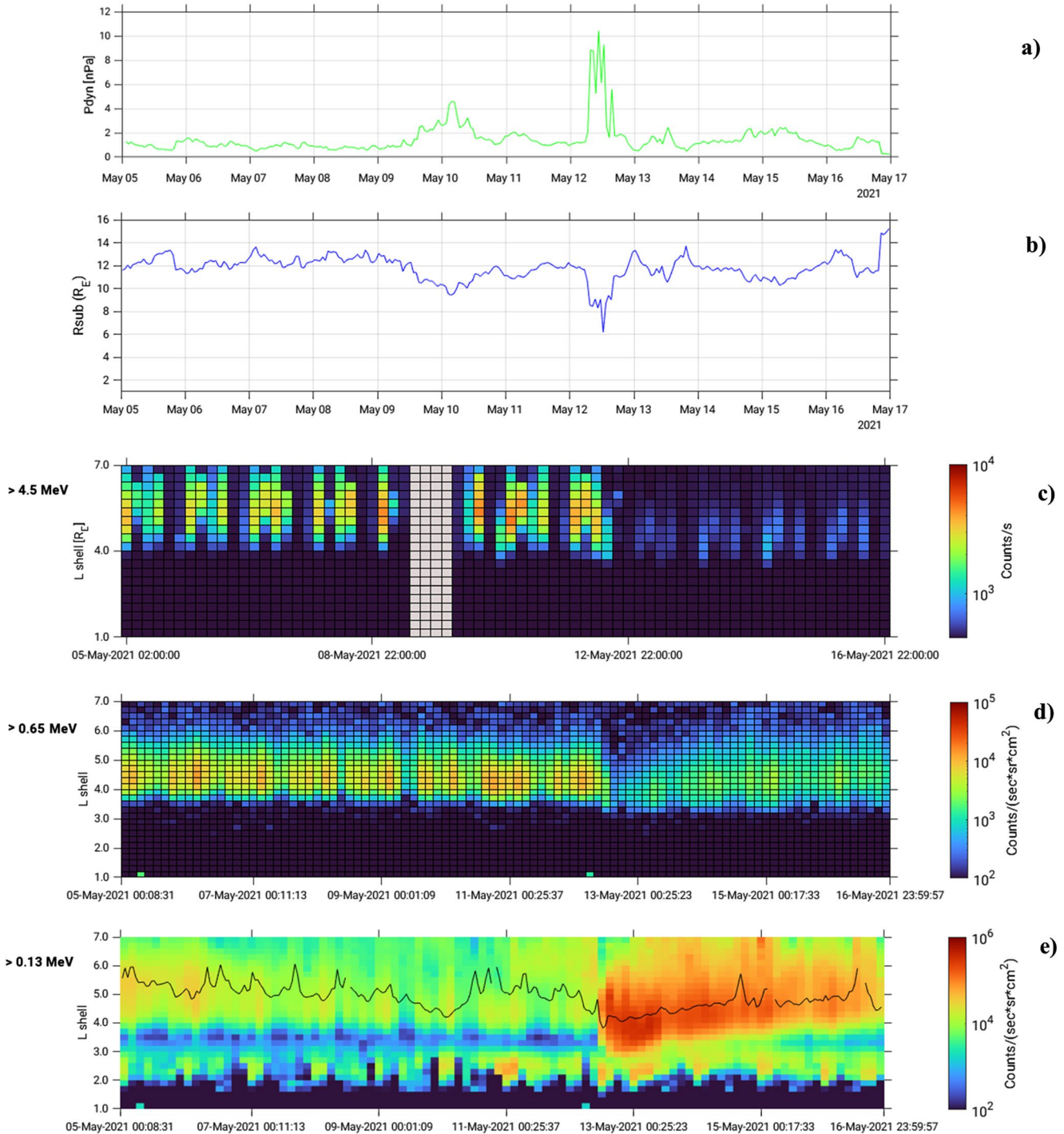


Figure 6. Panel (a): Time profile of the solar wind dynamic pressure (OMNI data magenta curve) and position of the magnetopause standoff distance (as estimated from the Shue et al. (1998) model, black curve) over the period of 5–16 May 2021; Panel (b): >0.13 MeV electron fluxes measured by MEPED-90° over the same period. The superimposed black line represents the position of the plasmaopause as estimated from the X. Liu and Liu (2014) model; Panel (c) >0.65 electron fluxes measured by the azimuthal MEPED-90° telescope on board the NOAA19 satellite over the same period; Panel (d): Rates of >4.5 MeV particles detected by High-Energy Particle Detector (HEPD-01) over the same period. Gray shaded areas refer to time intervals for which HEPD data are not available.

et al., 2016) and outward radial transport, as suggested by a deep incursion of the magnetopause, as estimated from the Shue et al. (1998) model, on L shells no higher (Case & Wild, 2013) than $\sim 6.2 R_E$ in correspondence with the peak of the storm (Figure 6a). Further considerations about the role of magnetopause shadowing in the May 2021 storm event are reported in Section 4.

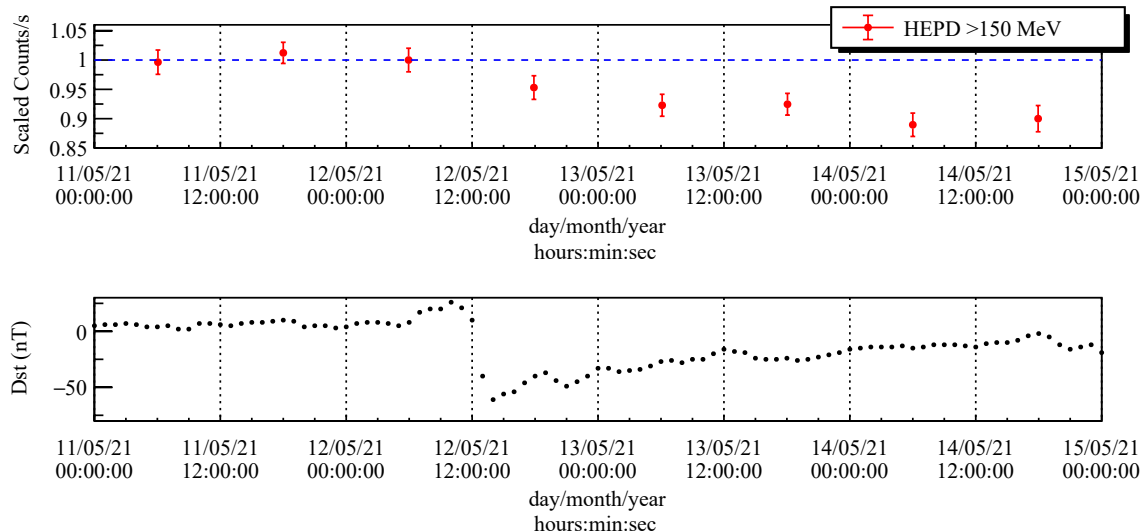


Figure 7. 12-hr averaged galactic cosmic-ray (GCR) proton intensity variation profile as a function of time from High-Energy Particle Detector (HEPD-01) observations in the >150 MeV energy range (top panel). A clear suppression of GCR intensity can be spotted after 12 May 2021 0600 UTC. At the same time, it is possible to see an abrupt variation in Dst index (bottom panel).

Forbush decreases (FDs) refer to sudden suppression of the short-term galactic cosmic-ray (GCR) intensity (Forbush, 1937; Hess & Demmelair, 1937), either associated with corotating high-speed streams (“recurrent” FDs) or caused by transient solar wind structures following coronal mass ejections from the Sun (“non-recurrent” FDs). Most of the early observations of such phenomena were carried out by ground-based detectors, such as Neutron Monitors and Muon Telescopes (Cane, 2000; Papailiou et al., 2020; Vieira et al., 2012), and by measurements with ionization chambers (Hayakawa, Oliveira, et al., 2021) allowing only for an indirect detection of the neutrons generated in the atmosphere. Figure 7 shows the variation of GCR protons measured by the HEPD-01 instrument, directly from space, across the storm and post-storm of May 2021. The 12-hr-averaged galactic protons intensity variation as a function of time has been studied in the >150 MeV energy range (red points in the top panel), selecting only particles at the very polar sectors of the CSES-01 orbit, where the geomagnetic cutoff is low enough to allow, in the absence of strong proton events (e.g., Piersanti et al., 2017; Tranquille, 1994), for galactic proton detection. The applied selection criteria were the same described in Bartocci et al. (2020). A clear suppression of GCR intensity after 12 May 2021 0600 UTC is evident, in conjunction with the arrival of the storm, as observed by the abrupt variations in Dst index (bottom panel). The overall maximum variation of the proton intensity profiles is around -10% .

The observations of cosmic ray variation during solar flares or CMEs provide constraints on the acceleration mechanisms and magnetic reconnection processes operative in the flares. CMEs and the shocks they drive cause FDs, and since the same phenomena are also responsible for geomagnetic storms, the study of the time-profiles of GCRs during such storms could provide valuable information about these space weather disturbances. Furthermore, certain phenomena associated with FDs, such as precursory decreases and spatial anisotropies can give advanced information regarding the intensity of geomagnetic storms themselves. For this reasons, it is important to have a detector that can study even small FDs (like the one reported in this work) with a sufficient precision and directly from space.

4. Discussion and Conclusions

The 12 May 2021 geomagnetic storm was caused by a CME occurred on 9 May 2021 at $t_0 = 11:30$ UT as a consequence of a filament eruption observed in the southern solar hemisphere, as recorded by SDO AIA imagers. Under the hypothesis of radial propagation, and de-projecting the CME velocity, we have estimated its radial velocity as $V_{rad} = (720 \pm 100)$ km/s. Observations by HI-1 confirmed such results, by imaging of the ICME at a larger distance from the Sun from the early hours of 10 May 2021 to late 11 May 2021 with a PoS velocity

of 500 km/s. It is interesting to note that, at the moment of the CME lift-off, a large CH (gray line in Figure 1) was present very close to the filament coordinates, leading to fast SW stream that very likely affected the CME propagation in the interplanetary space.

To reproduce the ICME behavior in the interplanetary space, we have used the P-DBM (Napoletano et al., 2018) model for the propagation of the CME in the heliosphere. Under the hypothesis that the part of the ICME hitting the Earth interacts with the fast SW generated by the CH over the whole duration of its travel, we have estimated its time travel to 1 AU and its velocity at arrival, obtaining 12 May 2021 at 04:00 ± 6h and 640 ± 70 km/s, respectively. Such estimations are confirmed by the observations at the first Lagrangian point (WIND satellite), which detected the ICME arrival on May 12 at 08:23 UT. The magnetic cloud was preceded by an interplanetary shock passing through the satellite at 05:56 UT. We have estimated both the shock normal orientation as $\Theta_{SE,W} \approx -177^\circ$ and $\Phi_{SE,W} \approx 111^\circ$, and the shock speed as $v_{sh,W} \approx 538$ km/s. Under the assumption of a planar propagation, we have obtained that the IPs impacted onto the magnetopause in the noon sector.

The consequence of the ICME passage through the Earth's magnetosphere was the reconfiguration of the magnetospheric principal current systems. At the moment of the arrival of the IPs, the magnetopause nose moved back to $\sim 6.8 R_E$, as a consequence of the concurrent contributions of a strong increase in the SW dynamic pressure and the southward switching of the IMF orientation (Lee & Lyons, 2004; Piersanti et al., 2020; Piersanti & Villante, 2016; Villante & Piersanti, 2011; Wang et al., 2009). As to the magnetospheric field observed at geosynchronous orbit, strong variations in both $B_{Z,GSE}$ and $B_{x,GSE}$ were detected. During the passage of the magnetic cloud, the magnetospheric field lines turned out strongly stretched and twisted. Indeed, geosynchronous observations showed: (a) a huge decrease along both the $B_{z,GSE}$ and $B_{x,GSE}$ in the local morning sector ($06:36 < LT_{G16} < 10:24$); (b) an increase then decrease along $B_{z,GSE}$ coupled with a large decrease in both $B_{x,GSE}$ and $B_{y,GSE}$ components in the local night sector ($02:36 < LT_{G17} < 06:24$). We interpreted those observations as the interplay of the activity of the partial ring current, which increased in amplitude due to the reconnection at the magnetopause, with the activity of the magnetotail current, which dipolarizes and experiences an increasing of plasma density in its neutral sheet caused by the passage of the magnetic cloud (A. T. Y. Lui, 2016; Murphy et al., 2022, and reference therein). Indeed, the direct comparison between GOES observations and an “ad hoc” modified Tsyganenko and Sitnov (2005) model predictions, confirms our explanation. In fact, the best representation of the magnetospheric field is given by the concurring contribution of the ring current and tail current alone, in which the hinging point is shifted Earthward (from $8.75R_E$ to $6.85R_E$) and the current sheet thickness has been increased from $5R_E$ to $5.9R_E$ (Dayeh et al., 2015; Kan, 1973; Thompson et al., 2005; Tsyganenko & Sitnov, 2005; Xiao et al., 2016). Such a magnetospheric current configuration is coherent with previous analysis and observations (Akasofu, 2020; Ghamry et al., 2016; Iyemori, 1990; Piersanti et al., 2017; Tsurutani et al., 2020).

A similar situation was observed in the ionosphere at ~ 500 km height, where the low frequency contributions (of magnetospheric origin), as obtained by the MA.I.GIC. model (Piersanti et al., 2019), were characterized by a strong decrease along the North-South direction during the main phase of the geomagnetic storm, and a long lasting increase during the recovery phase. On the other hand, the East-West component showed a negative, then positive, variation during both the main and the recovery phase of the geomagnetic storm. This was the clear consequence of the concurrent activities of both the asymmetric part of the ring current and tail current along $B_{N,LF}$ (Lühr & Zhou, 2020; Neubert et al., 2001; Park et al., 2020; Piersanti et al., 2020). This interpretation has been corroborated by the direct comparison between satellite observations and TS04* model predictions, which well represents the variations along both $B_{N,LF}$ and $B_{E,LF}$. The contribution of ionospheric origin (high-frequency components) showed larger variations along $B_{E,HF}$. This behavior can be explained in terms of the overlapping contributions from the ionospheric current system and magnetospheric-ionospheric coupling processes. Indeed, $B_{E,HF}$ showed a positive then negative variation during the main phase, likely as the consequence of the loading-unloading process between the magnetosphere and the ionosphere (Blockx et al., 2009; Consolini & De Michelis, 2005; Piersanti et al., 2017). At the same time, during the recovery phase, the ionospheric DP-2 current system (Brathwaite & Rostoker, 1981) clearly switched on as inferred by the huge positive variations observed in $B_{E,HF}$ (Nishida, 1968; Piersanti et al., 2020; Shinbori et al., 2013).

The redistribution of electrons in the Earth's magnetosphere has been monitored by means of data from particle detectors on board the NOAA19-POES and CSES-01 satellites (see Figure 6). We have verified that one primary impact of the storm development is the sudden and persistent loss of relativistic electrons from the entire ORB (L. Y. Li et al., 2009), whose very rapid, non-recovering dropout can only be the result of non-adiabatic processes

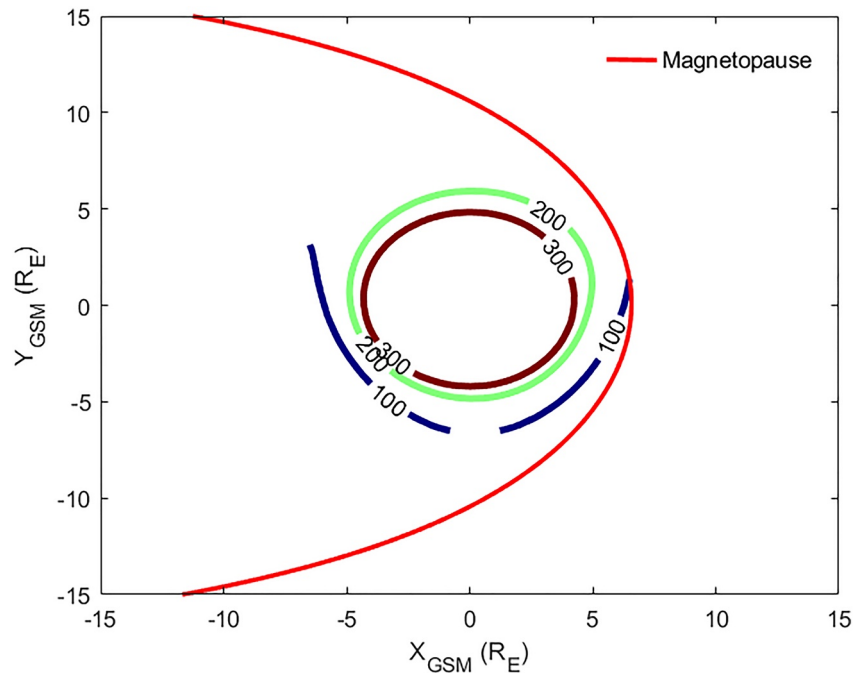


Figure 8. Equatorial GSM cuts of the TS04* modeled magnetosphere at the time of maximum compression. The red curve represents the location of the magnetopause boundary. The other colored lines represent the iso-contours of the local magnetic field strength over the 100–300 nT range.

permanently removing particles from the system. As previously mentioned, one of these processes can likely be the magnetopause shadowing (MS) in combination with outward radial transport, as suggested by the perfect match between the deep magnetopause incursion on sub-geostationary distances around 12:50 UTC of May 12 (Figure 6, panel a) and the abrupt ten-fold increment in solar wind dynamic pressure over the same time interval. Indeed, Gao et al. (2015) performed a POES/GOES/OMNI superposed epoch analysis of 193 relativistic-electron dropout events over 16 years, identifying the solar wind dynamic pressure and the north-south component of the interplanetary magnetic field as the main drivers of electron depletions in the ORB. In their study, while large solar wind dynamic pressure values are found to strongly push the magnetopause inward causing electrons to escape the magnetosphere, persistent southward interplanetary $B_{z,IMF}$ preferentially results in electron scattering into the loss cone and consequent (wave-driven) precipitation to the atmosphere. Further, we have performed a TS04* simulation of the Earth's magnetosphere at the exact time of minimum magnetopause distance, extracting X-Y GSM cuts that include the magnetopause location and the iso-contours of the local magnetic field strength over the 100–300 nT range (Figure 8). When MS is in action, ORB electrons are depleted on open drift paths that were previously closed (Kim et al., 2008; Turner et al., 2012). According to Sibeck et al. (1987) magnetic field iso-contours basically correspond to drift paths of equatorially mirroring (i.e., 90° pitch-angle) electrons that, at large L shell, are more likely to intercept the magnetopause and get lost. In Figure 8, the magnetopause intercepts the 100 nT line near the geosynchronous orbit at the time of maximum compression, which is strongly suggestive of MS having a role in removing relativistic electrons from the ORB. The dropouts observed by both MEPED-90° and HEPD-01 at relativistic energies penetrate down to $L \sim 4$, which is a value significantly lower than minimum magnetopause standoff distance. A recent model (Ukhorskiy et al., 2015) suggests that MS and outward radial transport should be sufficient to trigger such deep losses, even though this not rarely happens in concurrence with wave-induced precipitation to the atmosphere (Herrera et al., 2016). In addition, recent test-particle simulations in storm period (Ukhorskiy et al., 2006) address large diamagnetic effects from the enhancement of a partial ring current, which once again can result in violation of the third adiabatic invariant and prompt loss of ORB electrons to the magnetopause. The absence of long-lasting substorm activity completes the scenario, since earlier studies (Antonova et al., 2018; Jaynes et al., 2015) show a direct relationship between substorms and ORB electron replenishment during the storm's recovery phase.

Finally, we detected a small Forbush decrease analyzing energetic protons at 500 km height. Though no clear two-step profile can be associated to this structure, the FD timing is consistent with an interplay between the IP shock and subsequent magnetic cloud as the origin of the small modulation, in accordance with earlier statistical surveys on the subject (Sanderson et al., 1990; Zhang & Burlaga, 1988).

As a closing comment, we want to highlight that despite the Sun is in general more active during its maximum and declining phases, recent papers showed the occurrence of extreme space weather events close to the solar activity minimum (Hayakawa et al., 2020; Hayakawa, Schlegel, et al., 2021; Piersanti et al., 2020). As a consequence, we remark that this kind of global analysis - namely, the study of an ICME propagation from its source on the Sun across the magnetosphere-ionosphere system to its impact in terms of magnetic field changes and magnetospheric particle redistribution, is still the straightforward way available to understand the complex dynamics of the processes occurring in the circumterrestrial environment from a space weather point of view. This analysis is an attempt to contribute to the systematization of the information available for these complex events, in the wider context of advancing our understanding of the aspects that determine the geoeffectiveness of solar activity manifestations.

Data Availability Statement

This work made use of the data from CSES mission (<https://leos.ac.cn/#/home>).

Acknowledgments

The authors thank the two anonymous reviewers for their careful reading of our manuscript and their many insightful comments and suggestions. This work made use of data from the CSES mission, a project funded by the China National Space Administration and the China Earthquake Administration in collaboration with the Italian Space Agency and the Istituto Nazionale di Fisica Nucleare. The authors kindly acknowledge the NASA CDAWeb team for making these data available. We also acknowledge the NOAA Space Weather Prediction Center for providing POES/GOES data. The authors thank the Italian Space Agency for the financial support under the contract ASI “LIMADOU Scienza+” n° 2020-31-HH.0. M. Piersanti, and G. D’Angelo thank the ISSI-BJ project “The electromagnetic data validation and scientific application research based on CSES satellite” and Dragon 5 cooperation 2020–2024 (ID. 59236). A. Cicone is a member of the Italian “Gruppo Nazionale di Calcolo Scientifico” (GNCS) of the Istituto Nazionale di Alta Matematica “Francesco Severi” (INdAM). This research has been carried out in the framework of the CAESAR (Comprehensive sPace weAther Studies for the ASPIS prototype Realization) project, supported by the Italian Space Agency and the National Institute of Astrophysics through the ASI-INAf n.2020-35-HH.0 agreement for the development of the ASPIS (ASI SPace weather InfraStructure) prototype of scientific data centre for Space Weather.

References

- Akasofu, S.-I. (2020). Relationship between geomagnetic storms and auroral/magnetospheric substorms: Early studies. *Frontiers in Astronomy and Space Sciences*, 7, 101. <https://doi.org/10.3389/fspas.2020.604755>
- Antonova, E., Stepanova, M., Moya, P., Pinto, V., Vovchenko, V., Ovchinnikov, I., & Sotnikov, N. (2018). Processes in auroral oval and outer electron radiation belt. *Earth Planets and Space*, 70(1), 127. <https://doi.org/10.1186/s40623-018-0898-1>
- Baker, D. N., Erickson, P. J., Fennell, J. F., Foster, J. C., Jaynes, A. N., & Verronen, P. T. (2018). Space weather effects in the Earth’s radiation belts. *Space Science Reviews*, 214(1), 17. <https://doi.org/10.1007/s11214-017-0452-7>
- Baker, D. N., Jaynes, A. N., Hoxie, V. C., Thorne, R. M., Foster, J. C., Li, X., et al. (2014). An impenetrable barrier to ultrarelativistic electrons in the van Allen radiation belts. *Nature*, 515(7528), 531–534. <https://doi.org/10.1038/nature13956>
- Baker, D. N., Jaynes, A. N., Kanekal, S. G., Foster, J. C., Erickson, P. J., Fennell, J. F., et al. (2016). Highly relativistic radiation belt electron acceleration, transport, and loss: Large solar storm events of March and June 2015. *Journal of Geophysical Research: Space Physics*, 121(7), 6647–6660. <https://doi.org/10.1002/2016JA022502>
- Baker, D. N., Kanekal, S. G., Hoxie, V. C., Batiste, S., Bolton, M., Li, X., et al. (2013). The relativistic electron-proton telescope (REPT) instrument on board the radiation belt storm probes (RBSP) spacecraft: Characterization of Earth’s radiation belt high-energy particle populations. *Space Science Reviews*, 179(1–4), 337–381. <https://doi.org/10.1007/s11214-012-9950-9>
- Barnes, D., Davies, J., Harrison, R., Byrne, J., Perry, C., Bothmer, V., et al. (2019). CMes in the heliosphere: II. A statistical analysis of the kinematic properties derived from single-spacecraft geometrical modelling techniques applied to CMes detected in the heliosphere from 2007 to 2017 by stereo/hi-1. *Solar Physics*, 05294(5), 57. <https://doi.org/10.1007/s11207-019-1444-4>
- Bartocci, S., Battiston, R., Burger, W. J., Campana, D., Carfora, L., Castellini, G., et al. (2020). Galactic cosmic-ray hydrogen spectra in the 40–250 MeV range measured by the high-energy particle detector (HEPD) on board the CSES-01 satellite between 2018 and 2020. *The Astrophysical Journal*, 901(1), 8. <https://doi.org/10.3847/1538-4357/ab4d3e>
- Blake, J. B., Carranza, P. A., Claudepierre, S. G., Clemmons, J. H., Crain, W. R., Dotan, Y., et al. (2013). The magnetic electron ion spectrometer (MagEIS) instruments aboard the radiation belt storm probes (RBSP) spacecraft. *Space Science Reviews*, 179(1–4), 383–421. <https://doi.org/10.1007/s11214-013-9991-8>
- Blockx, C., Gérard, J.-C., Coumans, V., Hubert, B., & Meurant, M. (2009). Contributions of the driven process and the loading-unloading process during substorms: A study based on the image-Si1₂ imager. *Journal of Geophysical Research*, 114(A2). <https://doi.org/10.1029/2008JA013280>
- Boteler, D. H. (2019). A 21st century view of the March 1989 magnetic storm. *Space Weather*, 17(10), 1427–1441. <https://doi.org/10.1029/2019SW002278>
- Brathwaite, K., & Rostoker, G. (1981). Dp₂ current system in the ionosphere and magnetosphere. *Planetary and Space Science*, 29(5), 485–494. [https://doi.org/10.1016/0032-0633\(81\)90063-5](https://doi.org/10.1016/0032-0633(81)90063-5)
- Brueckner, G. E., Howard, R. A., Koomen, M. J., Korendyke, C. M., Michels, D. J., Moses, J. D., et al. (1995). The large angle spectroscopic Coronagraph (LASCO). *Solar Physics*, 162(1–2), 357–402. <https://doi.org/10.1007/BF00733434>
- Burlaga, L., Sittler, E., Mariani, F., & Schwenn, R. (1981). Magnetic loop behind an interplanetary shock: Voyager, Helios, and Imp 8 observations. *Journal of Geophysical Research*, 86(A8), 6673–6684. <https://doi.org/10.1029/JA086iA08p06673>
- Cane, H. V. (2000). Coronal mass ejections and forrush decreases. *Space Science Reviews*, 93(1), 55–77. <https://doi.org/10.1023/A:1026532125747>
- Cargill, P. J. (2004). On the aerodynamic drag force acting on interplanetary coronal mass ejections. *Solar Physics*, 221(1), 135–149. <https://doi.org/10.1023/b:sola.0000033366.10725.a2>
- Carter, B. A., Yizengaw, E., Pradipta, R., Weygand, J. M., Piersanti, M., Pulkkinen, A., et al. (2016). Geomagnetically induced currents around the world during the 17 March 2015 storm. *Journal of Geophysical Research: Space*, 121(10), 10496–10507. 2016JA023344. <https://doi.org/10.1002/2016JA023344>
- Case, N. A., & Wild, J. A. (2013). The location of the Earth’s magnetopause: A comparison of modeled position and in situ cluster data. *Journal of Geophysical Research: Space Physics*, 118(10), 6127–6135. <https://doi.org/10.1002/jgra.50572>

- Cliver, E. W., & Dietrich, W. F. (2013). The 1859 space weather event revisited: Limits of extreme activity. *Journal of Space Weather Space Climate*, 3, A31. <https://doi.org/10.1051/swsc/2013053>
- Consolini, G., & De Michelis, P. (2005). Local intermittency measure analysis of ae index: The directly driven and unloading component. *Geophysical Research Letters*, 32(5), L05101. <https://doi.org/10.1029/2004GL022063>
- Dayeh, M. A., Fuselier, S. A., Funsten, H. O., McComas, D. J., Ogasawara, K., Petrinc, S. M., et al. (2015). Shape of the terrestrial plasma sheet in the near-Earth magnetospheric tail as imaged by the interstellar boundary explorer. *Geophysical Research Letters*, 42(7), 2115–2122. <https://doi.org/10.1002/2015GL063682>
- Del Moro, D., Napoletano, G., Forte, R., Giovannelli, L., Pietropaolo, E., & Berrilli, F. (2019). Forecasting the 2018 February 12th CME propagation with the p-dbm model: A fast warning procedure. *Annals of Geophysics*, 62(4), 456. <https://doi.org/10.4401/ag-7750>
- Domingo, V., Fleck, B., & Poland, A. I. (1995). The SOHO mission: An overview. *Solar Physics*, 162(1–2), 1–37. <https://doi.org/10.1007/BF00733425>
- Dyer, C., Hands, A., Ryden, K., & Lei, F. (2018). Extreme atmospheric radiation environments and single event effects. *IEEE Transactions on Nuclear Science*, 65(1), 432–438. <https://doi.org/10.1109/TNS.2017.2761258>
- Evans, D., & Greer, M. (2004). *Polar orbiting environmental satellite space environment monitor-2 instrument descriptions and archive data documentation*. NOAA Tech. Mem. 1.4. Space Environment Lab. Retrieved from <https://ngdc.noaa.gov/stp/satellite/poses/docs/SEM2Archive.pdf>
- Eyles, C., Harrison, R., Davis, C. J., Waltham, N., Shaughnessy, B., Mapson-Menard, H., et al. (2009). The heliospheric imagers onboard the stereo mission. *Solar Physics*, 254(2), 387–445. <https://doi.org/10.1007/s11207-008-9299-0>
- Finlay, C. C., Kloss, C., Olsen, N., Hammer, M. D., Tøffner-Clausen, L., Grayver, A., & Kuvshinov, A. (2020). The chaos-7 geomagnetic field model and observed changes in the South Atlantic anomaly. *Earth Planets and Space*, 72(1), 1–31. <https://doi.org/10.1186/s40623-020-01252-9>
- Forbush, S. E. (1937). On the effects in cosmic-ray intensity observed during the recent magnetic storm. *Physics Review*, 51(12), 1108–1109. <https://doi.org/10.1103/PhysRev.51.1108.3>
- Gao, X., Li, W., Bortnik, J., Thorne, R. M., Lu, Q., Ma, Q., et al. (2015). The effect of different solar wind parameters upon significant relativistic electron flux dropouts in the magnetosphere. *Journal of Geophysical Research: Space Physics*, 120(6), 4324–4337. <https://doi.org/10.1002/2015JA021182>
- Garcia, H. A., & Dryer, M. (1987). The solar flares of February 1986 and the ensuing intense geomagnetic storm. *Solar Physics*, 109(1), 119–137. <https://doi.org/10.1007/bf00167403>
- Ghamry, E., Lethy, A., Arafa-Hamed, T., & Abd Elaal, E. (2016). A comprehensive analysis of the geomagnetic storms occurred during 18 February and 2 March 2014. *NRIAG Journal of Astronomy and Geophysics*, 5(1), 263–268. <https://doi.org/10.1016/j.nrjag.2016.03.001>
- Gonzalez, W. D., Joselyn, J. A., Kamide, Y., Kroehl, H. W., Rostoker, G., Tsurutani, B. T., & Vasyliunas, V. M. (1994). What is a geomagnetic storm? *Journal of Geophysical Research: Space*, 99(A4), 5771–5792. <https://doi.org/10.1029/93JA02867>
- Gosling, J. T., Bame, S. J., McComas, D. J., & Phillips, J. L. (1990). Coronal mass ejections and large geomagnetic storms. *Geophysical Research Letters*, 17(7), 901–904. <https://doi.org/10.1029/GL017i007p00901>
- Hayakawa, H., Ebihara, Y., Willis, D. M., Toriumi, S., Iju, T., Hattori, K., et al. (2019). Temporal and spatial evolutions of a large sunspot group and great auroral storms around the Carrington event in 1859. *Space Weather*, 17(11), 1553–1569. <https://doi.org/10.1029/2019SW002269>
- Hayakawa, H., Hattori, K., Pevtsov, A. A., Ebihara, Y., Shea, M. A., McCracken, K. G., et al. (2021). The intensity and evolution of the extreme solar and geomagnetic storms in 1938 January. *The Astrophysical Journal*, 909(2), 197. <https://doi.org/10.3847/1538-4357/abc427>
- Hayakawa, H., Oliveira, D. M., Shea, M. A., Smart, D. F., Blake, S. P., Hattori, K., & Ebihara, Y. (2021). *The Extreme Solar and Geomagnetic Storms on 20–25 March 1940* (Vol. 12). Monthly Notices of the Royal Astronomical Society. [https://doi.org/10.1093/mnras/stab3615\(stab3615](https://doi.org/10.1093/mnras/stab3615(stab3615)
- Hayakawa, H., Ribeiro, P., Vaquero, J. M., Gallego, M. C., Knipp, D. J., Mekhaldi, F., et al. (2020). The extreme space weather event in 1903 October/November: An outburst from the quiet sun. *The Astrophysical Journal Letters*, 897(1), L10. <https://doi.org/10.3847/2041-8213/ab6a18>
- Hayakawa, H., Schlegel, K., Besser, B. P., & Ebihara, Y. (2021). Candidate auroral observations indicating a major solar–terrestrial storm in 1680: Implication for space weather events during the maunder minimum. *The Astrophysical Journal*, 909(1), 29.
- Herrera, D., Maget, V. F., & Sicard-Piet, A. (2016). Characterizing magnetopause shadowing effects in the outer electron radiation belt during geomagnetic storms. *Journal of Geophysical Research: Space Physics*, 121(10), 9517–9530. <https://doi.org/10.1002/2016JA022825>
- Hess, V. F., & Demmelmair, A. (1937). August) world-wide effect in cosmic ray intensity, as observed during a recent magnetic storm. *Nature*, 140(3538), 316–317. <https://doi.org/10.1038/140316a0>
- Howard, R. A., Moses, J. D., Vourlidas, A., Newmark, J. S., Socker, D. G., Plunkett, S. P., et al. (2008). April). Sun Earth Connection coronal and heliospheric investigation (SECCHI). *Space Science Reviews*, 136(1–4), 67–115. <https://doi.org/10.1007/s11214-008-9341-4>
- Iyemori, T. (1990). Storm-time magnetospheric currents inferred from mid-latitude geomagnetic field variations. *Journal of Geomagnetism and Geoelectricity*, 42(11), 1249–1265. <https://doi.org/10.5636/jgg.42.1249>
- Jaynes, A. N., Baker, D. N., Singer, H. J., Rodriguez, J. V., Loto'aniu, T. M., Ali, A. F., et al. (2015). Source and seed populations for relativistic electrons: Their roles in radiation belt changes. *Journal of Geophysical Research: Space Physics*, 120(9), 7240–7254. <https://doi.org/10.1002/2015JA021234>
- Kaiser, M. L., Kucera, T. A., Davila, J. M., Cyr, S. O. C., Guhathakurta, M., & Christian, E. (2008). The STEREO mission: An introduction. *Space Science Reviews*, 136(1–4), 5–16. <https://doi.org/10.1007/s11214-007-9277-0>
- Kalegaev, V., Ganushkina, N. Y., Pulkkinen, T., Kubyshkina, M., Singer, H., & Russell, C. (2005). Relation between the ring current and the tail current during magnetic storms. *Annales Geophysicae*, 23(2), 523–533. <https://doi.org/10.5194/angeo-23-523-2005>
- Kamide, Y. (1988). Estimate of electromagnetic quantities in space from ground magnetic records. *Science*, 241(4863), 328–330. <https://doi.org/10.1126/science.241.4863.328>
- Kamide, Y., McPherron, R. L., Gonzalez, W. D., Hamilton, D. C., Hudson, H. S., Joselyn, J. A., & Szuszczewicz, E. (1997). Magnetic storms: Current understanding and outstanding questions. In *Magnetic storms* (pp. 1–19). American Geophysical Union (AGU). <https://doi.org/10.1029/GM098p0001>
- Kan, J. R. (1973). On the structure of the magnetotail current sheet. *Journal of Geophysical Research*, 78(19), 3773–3781. <https://doi.org/10.1029/JA078i019p03773>
- Khoo, L. Y., Li, X., Zhao, H., Sarris, T. E., Xiang, Z., Zhang, K., et al. (2018). On the initial enhancement of energetic electrons and the innermost plasma pause locations: Coronal mass ejection-driven storm periods. *Journal of Geophysical Research: Space Physics*, 123(11), 9252–9264. <https://doi.org/10.1029/2018ja026074>
- Kim, K., Lee, D., Kim, H., Lyons, L., Lee, E., Oeztuerk, M., & Choi, C. (2008). Numerical calculations of relativistic electron drift loss effect. *Journal of Geophysical Research*, 113(A9), A09212. <https://doi.org/10.1029/2007JA013011>
- Kivelson, M. G., Kivelson, M. G., & Russell, C. T. (1995). *Introduction to space physics*. Cambridge University Press.
- Knipp, D. J., Bernstein, V., Wahl, K., & Hayakawa, H. (2021). Timelines as a tool for learning about space weather storms. *Journal of Space Weather Space Climate*, 11, 29. <https://doi.org/10.1051/swsc/2021011>

- Knipp, D. J., Fraser, B. J., Shea, M. A., & Smart, D. F. (2018). On the little-known consequences of the 4 August 1972 ultra-fast coronal mass ejecta: Facts, commentary, and call to action. *Space Weather*, *16*(11), 1635–1643. <https://doi.org/10.1029/2018SW002024>
- Koskinen, H. E., Baker, D. N., Balogh, A., Gombosi, T., Veronig, A., & von Steiger, R. (2017). Achievements and challenges in the science of space weather. *Space Science Reviews*, *212*(3), 1137–1157. https://doi.org/10.1007/978-94-024-1588-9_1
- Landau, L. D., Bell, J., Kearsley, M., Pitaevskii, L., Lifshitz, E., & Sykes, J. (1960). *Electrodynamics of Continuous Media* (Vol. 8). Elsevier.
- Lanzerotti, L. J. (2001). Space weather effects on communications. In I. A. Daglis (Ed.), *Space storms and space weather hazards* (pp. 313–334). Springer Netherlands. https://doi.org/10.1007/978-94-010-0983-6_12
- Lanzerotti, L. J. (2017). Space weather: Historical and contemporary perspectives. *Space Science Reviews*, *212*(3), 1253–1270. <https://doi.org/10.1007/s11214-017-0408-y>
- Lee, D.-Y., & Lyons, L. R. (2004). Geosynchronous magnetic field response to solar wind dynamic pressure pulse. *Journal of Geophysical Research*, *109*(A4). <https://doi.org/10.1029/2003JA010076>
- Lemen, J. R., Title, A. M., Akin, D. J., Boerner, P. F., Chou, C., Drake, J. F., et al. (2012). Waltham, NJ (January). The atmospheric imaging assembly (AIA) on the solar dynamics observatory (SDO). *Solar Physics*, *275*(1–2), 17–40. <https://doi.org/10.1007/s11207-011-9776-8>
- Lepping, R. P., Acuña, M. H., Burlaga, L. F., Farrell, W. M., Slavin, J. A., Schatten, K. H., et al. (1995). The wind magnetic field investigation. *Space Science Reviews*, *71*(1–4), 207–229. <https://doi.org/10.1007/BF00751330>
- Li, L. Y., Cao, J. B., Zhou, G. C., & Li, X. (2009). Statistical roles of storms and substorms in changing the entire outer zone relativistic electron population. *Journal of Geophysical Research*, *114*(A12), A12214. <https://doi.org/10.1029/2009JA014333>
- Li, W., Thorne, R. M., Ma, Q., Ni, B., Bortnik, J., Baker, D. N., et al. (2014). Radiation belt electron acceleration by chorus waves during the 17 March 2013 storm. *Journal of Geophysical Research: Space Physics*, *119*(6), 4681–4693. <https://doi.org/10.1002/2014JA019945>
- Liu, W., & Cao, J. (2014). Effect of plasmopause on the generation of ultra low frequency (ULF) waves. *XXXIth URSI General Assembly and Scientific Symposium*, 1. <https://doi.org/10.1109/ursigass.2014.6929949>
- Liu, X., & Liu, W. (2014). A new plasmopause location model based on themis observations. *Science in China—Series D: Earth Sciences*, *57*(10), 2552–2557. <https://doi.org/10.1007/s11430-014-4844-1>
- Liu, Y. D., Zhao, X., Hu, H., Vourlidis, A., & Zhu, B. (2019). A comparative study of 2017 July and 2012 July complex eruptions: Are solar superstorms “perfect storms” in nature? *The Astrophysical Journal—Supplement Series*, *241*(2), 15. <https://doi.org/10.3847/1538-4365/ab0649>
- Lühr, H., & Zhou, Y.-L. (2020). Relation between the asymmetric ring current effect and the anti-sunward auroral currents, as deduced from champ observations. *Annales Geophysicae*, *38*(3), 749–764. <https://doi.org/10.5194/angeo-38-749-2020>
- Lui, A., Chapman, S., Liou, K., Newell, P., Meng, C., Brittnacher, M., & Parks, G. (2000). Is the dynamic magnetosphere an avalanching system? *Geophysical Research Letters*, *27*(7), 914. <https://doi.org/10.1029/1999gl010752>
- Lui, A. T. Y. (2016). Dipolarization front and current disruption. *Geophysical Research Letters*, *43*(19), 10. <https://doi.org/10.1002/2016GL070980>
- McIlwain, C. E. (1961). Coordinates for mapping the distribution of magnetically trapped particles. *Journal of Geophysical Research*, *66*(11), 3681–3691. <https://doi.org/10.1029/JZ066i011p03681>
- Meng, X., Tsurutani, B. T., & Mannucci, A. J. (2019). The solar and interplanetary causes of superstorms (minimum $dst \leq -250$ nt) during the space age. *Journal of Geophysical Research: Space Physics*, *124*(6), 3926–3948. <https://doi.org/10.1029/2018JA026425>
- Milan, S. E., Clausen, L. B. N., Coxon, J. C., Carter, J. A., Walach, M.-T., Laundal, K., et al. (2017). Overview of solar wind–magnetosphere–ionosphere–atmosphere coupling and the generation of magnetospheric currents. *Space Science Reviews*, *206*(1), 547–573. <https://doi.org/10.1007/s11214-017-0333-0>
- Miyake, F., Usoskin, I., & Polunin, S. (2019). Extreme solar particle storms. *The hostile Sun*. <https://doi.org/10.1088/2514-3433/ab404a>
- Murphy, K. R., Bentley, S. N., Miles, D. M., Sandhu, J. K., & Smith, A. W. (2022). Chapter 7—Imaging the magnetosphere–ionosphere system with ground-based and in-situ magnetometers. In Y. Colado-Vega, D. Gallagher, H. Frey, & S. Wing (Eds.), *Understanding the space environment through global measurements* (pp. 287–340). Elsevier. <https://doi.org/10.1016/B978-0-12-820630-0.00002-7>
- Napoletano, G., Folds, R., Berrilli, F., Camporeale, E., de Gasperis, G., Giovannelli, L., & Del Moro, D. (2021). *Parameter distributions for the drag-based modeling of cme propagation*. Space Weather.
- Napoletano, G., Forte, R., Del Moro, D., Pietropaolo, E., Giovannelli, L., & Berrilli, F. (2018). A probabilistic approach to the drag-based model. *Journal of Space Weather Space Climate*, *8*, A11. <https://doi.org/10.1051/swsc/2018003>
- Navia, C. E., de Oliveira, M. N., & Augusto, C. R. A. (2018). The highest geomagnetic storms of the solar cycle observed at ground level. In P. J. Sallis (Ed.), *Extreme weather*. IntechOpen. (Vol. 3). <https://doi.org/10.5772/intechopen.75688>
- Neubert, T., Manda, M., Hulot, G., von Frese, R., Primdahl, F., Jørgensen, J. L., et al. (2001). Ørsted satellite captures high-precision geomagnetic field data. *Eos, Transactions American Geophysical Union*, *82*(7), 81–88. <https://doi.org/10.1029/01EO00043>
- Nishida, A. (1968). Coherence of geomagnetic Dp 2 fluctuations with interplanetary magnetic variations. *Journal of Geophysical Research*, *73*(17), 5549–5559. <https://doi.org/10.1029/JA073i017p05549>
- Ohtani, S., Ebihara, Y., & Singer, H. J. (2007). Storm-time magnetic configurations at geosynchronous orbit: Comparison between the main and recovery phases. *Journal of Geophysical Research*, *112*(A5). <https://doi.org/10.1029/2006JA011959>
- Oliveira, D. (2017). Magnetohydrodynamic shocks in the interplanetary space: A theoretical review. *Brazilian Journal of Physics*, *47*(1), 81–95. <https://doi.org/10.1007/s13538-016-0472-x>
- Palma, F., Sotgiu, A., Parmentier, A., Martucci, M., Piersanti, M., Bartocci, S., et al. (2021). The August 2018 geomagnetic storm observed by the high-energy particle detector on board the CSES-01 satellite. *Applied Sciences*, *11*(12), 5680. <https://doi.org/10.3390/app11125680>
- Papailiou, M., Abunina, M., Belov, A., Eroshenko, E., Yanke, V., & Mavromichalaki, H. (2020). Large forrush decreases and their solar sources: Features and characteristics. *Solar Physics*, *295*(12), 1–13. <https://doi.org/10.1007/s11207-020-01735-8>
- Park, J., Stolle, C., Yamazaki, Y., Rauberg, J., Michaelis, I., & Olsen, N. (2020). Diagnosing low-/mid-latitude ionospheric currents using platform magnetometers: Cryosat-2 and grace-fo. *Earth Planets and Space*, *72*(1), 1–18. <https://doi.org/10.1186/s40623-020-01274-3>
- Pesnell, W. D., Thompson, B. J., & Chamberlin, P. (2011). The solar dynamics observatory (SDO). In *The solar dynamics observatory* (pp. 3–15). Springer.
- Picozza, P., Battiston, R., Ambrosi, G., Bartocci, S., Basara, L., Burger, W. J., et al. (2019). Scientific goals and in-orbit performance of the high-energy particle detector on board the CSES. *The Astrophysical Journal—Supplement Series*, *243*(1), 16. <https://doi.org/10.3847/1538-4365/ab276c>
- Piersanti, M., Alberti, T., Bemporad, A., Berrilli, F., Bruno, R., Capparelli, V., et al. (2017). Comprehensive analysis of the geoeffective solar event of 21 June 2015: Effects on the magnetosphere, plasmasphere, and ionosphere systems. *Solar Physics*, *292*(11), 169. <https://doi.org/10.1007/s11207-017-1186-0>
- Piersanti, M., De Michelis, P., Del Moro, D., Tozzi, R., Pezzopane, M., Consolini, G., et al. (2020). From the Sun to Earth: Effects of the 25 August 2018 geomagnetic storm. *Annales Geophysicae*, *38*(3), 703–724. <https://doi.org/10.5194/angeo-38-703-2020>

- Piersanti, M., Di Matteo, S., Carter, B. A., Currie, J., & D'Angelo, G. (2019). Geoelectric field evaluation during the September 2017 geomagnetic storm: Ma.i.gic. model. *Space Weather*, 17(8), 1241–1256. <https://doi.org/10.1029/2019SW002202>
- Piersanti, M., & Villante, U. (2016). On the discrimination between magnetospheric and ionospheric contributions on the ground manifestation of sudden impulses. *Journal of Geophysical Research: Space*, 121(7), 6674–6691. <https://doi.org/10.1002/2015JA021666>
- Plainaki, C., Antonucci, M., Bemporad, A., Berrilli, F., Bertucci, B., Castronuovo, M., et al. (2020). Current state and perspectives of space weather science in Italy. *Journal of Space Weather Space Climate*, 10, 6. <https://doi.org/10.1051/swsc/2020003>
- Pulkkinen, A., Bernabeu, E., Thomson, A., Viljanen, A., Pirjola, R., Boteler, D., et al. (2017). Geomagnetically induced currents: Science, engineering, and applications readiness. *Space Weather*, 15(7), 828–856. <https://doi.org/10.1002/2016SW001501>
- Pulkkinen, T. I., Ganushkina, N. Y., Tanskanen, E. I., Kubyshkina, M., Reeves, G. D., Thomsen, M. F., et al. (2006). Magnetospheric current systems during stormtime sawtooth events. *Journal of Geophysical Research*, 111(A11). <https://doi.org/10.1029/2006JA011627>
- Reyes, P., Pinto, V. A., & Moya, P. S. (2019). Statistical analysis of geomagnetic storms and their relation with the solar cycle. *Proceedings of the International Astronomical Union*, 15(S354), 224–227. <https://doi.org/10.1017/S1743921320000903>
- Riley, P., Baker, D., Liu, Y. D., Veron, P., Singer, H., & Güdel, M. (2018). Extreme space weather events: From cradle to grave. *Space Science Reviews*, 214(1), 1–24. https://doi.org/10.1007/978-94-024-1588-9_14
- Sanderson, T. R., Beeck, J., Marsden, R. G., Tranquille, C., Wenzel, K.-P., McKibben, R. B., & Smith, E. J. (1990). A study of the relation between magnetic clouds and forrush decreases. *Proceedings of the 21st International Cosmic Ray Conference*, 6, 251.
- Shen, X., Zong, Q.-G., & Zhang, X. (2018). Introduction to special section on the China seismo-electromagnetic satellite and initial results. *Earth and Planetary Physics*, 2(6), 439–443. <https://doi.org/10.26464/epp2018041>
- Shinbori, A., Hori, T., Tanaka, Y., Koyama, Y., Kikuchi, T., & Nagatsuma, T. (2013). Global distributions of storm-time ionospheric currents as seen in geomagnetic field variations. *Advances in Polar Sciences*, 24(4), 296–314. <https://doi.org/10.3724/SPJ.1085.2013.00296>
- Shue, J.-H., Song, P., Russell, C. T., Steinberg, J. T., Chao, J. K., Zastenker, G., et al. (1998). Magnetopause location under extreme solar wind conditions. *Journal of Geophysical Research*, 103(A8), 17691–17700. <https://doi.org/10.1029/98JA01103>
- Sibeck, D. G., McEntire, R. W., Lui, A. T. Y., Lopez, R. E., & Krimigis, S. M. (1987). Magnetic field drift shell splitting: Cause of unusual dayside particle pitch angle distributions during storms and substorms. *Journal of Geophysical Research*, 92(A12), 485–497. <https://doi.org/10.1029/ja092ia12p13485>
- Sitnov, M., Sharma, A., Papadopoulos, K., & Vassiliadis, D. (2001). Modeling substorm dynamics of the magnetosphere: From self-organization and self-organized criticality to nonequilibrium phase transitions. *Physical Review E*, 65(1), 016116. <https://doi.org/10.1103/physreve.65.016116>
- Thompson, S. M., Kivelson, M. G., Khurana, K. K., McPherron, R. L., Weygand, J. M., Balogh, A., & Kistler, L. M. (2005). Dynamic Harris current sheet thickness from cluster current density and plasma measurements. *Journal of Geophysical Research*, 110(A2). <https://doi.org/10.1029/2004JA010714>
- Tranquille, C. (1994). Solar proton events and their effect on space systems. *Radiation Physics and Chemistry*, 43(1), 35–45. [https://doi.org/10.1016/0969-806X\(94\)90200-3](https://doi.org/10.1016/0969-806X(94)90200-3)
- Tsurutani, B. T., Lakhina, G. S., & Hajra, R. (2020). The physics of space weather/solar-terrestrial physics (STP): What we know now and what the current and future challenges are. *Nonlinear Processes in Geophysics*, 27(1), 75–119. <https://doi.org/10.5194/npg-27-75-2020>
- Tsurutani, B. T., & Zhou, X.-Y. (2003). Interplanetary shock triggering of substorms: Wind and polar. *Advances in Space Research*, 31(4), 1063–1067. [https://doi.org/10.1016/s0273-1177\(02\)00796-2](https://doi.org/10.1016/s0273-1177(02)00796-2)
- Tsyganenko, N. A., & Sitnov, M. I. (2005). Modeling the dynamics of the inner magnetosphere during strong geomagnetic storms. *Journal of Geophysical Research: Space*, 110(A3), A03208. <https://doi.org/10.1029/2004JA010798>
- Turner, D., O'Brien, T., Fennell, J., Claudepierre, S., Bleake, J. E. K., & Hietala, H. (2015). The effects of geomagnetic storms on electrons in Earth's radiation belts. *Geophysical Research Letters*, 42(21), 9176–9184. <https://doi.org/10.1002/2015GL064747>
- Turner, D., Shprits, Y., Hartinger, M., & Angelopoulos, V. (2012). Explaining sudden losses of outer radiation belt electrons during geomagnetic storms. *Nature Physics*, 8(3), 208–212. <https://doi.org/10.1038/nphys2185>
- Ukhorskiy, A. Y., Anderson, B. J., Brandt, P., & Tsyganenko, N. (2006). Storm time evolution of the outer radiation belt: Transport and losses. *Journal of Geophysical Research*, 111(A11), A11S03. <https://doi.org/10.1029/2006JA011690>
- Ukhorskiy, A. Y., Sitnov, M. I., Millan, R. M., Kress, B. T., Fennell, J. F., Claudepierre, S. G., & Barnes, R. J. (2015). Global storm time depletion of the outer electron belt. *Journal of Geophysical Research: Space Physics*, 120(4), 2543–2556. <https://doi.org/10.1002/2014ja020645>
- Vieira, L. R., Lago, A. D., Rigozo, N. R., da Silva, M. R., Braga, C. R., Petry, A., & Schuch, N. J. (2012). Near 13.5-day periodicity in muon detector data during late 2001 and early 2002. *Advances in Space Research*, 49(11), 1615–1622. <https://doi.org/10.1016/j.asr.2012.01.017>
- Villante, U., & Piersanti, M. (2011). Sudden impulses at geosynchronous orbit and at ground. *Journal of Atmospheric and Solar-Terrestrial Physics*, 73(1), 61–76. <https://doi.org/10.1016/j.jastp.2010.01.008>
- Vršnak, B., Žic, T., Vrbanec, D., Temmer, M., Rollett, T., Möstl, C., et al. (2013). Propagation of interplanetary coronal mass ejections: The drag-based model. *Solar Physics*, 285(1–2), 295–315. <https://doi.org/10.1007/s11207-012-0035-4>
- Wang, C., Liu, J. B., Li, H., Huang, Z. H., Richardson, J. D., & Kan, J. R. (2009). Geospace magnetic field responses to interplanetary shocks. *Journal of Geophysical Research*, 114(A5). <https://doi.org/10.1029/2008JA013794>
- Willis, D. M., & Stephenson, F. R. (2000). Simultaneous auroral observations described in the historical records of China, Japan and Korea from ancient times to ad 1700. *Annales Geophysicae*, 18(1), 1–10. <https://doi.org/10.1007/s00585-000-0001-6>
- Xiao, S., Zhang, T., Ge, Y., Wang, G., Baumjohann, W., & Nakamura, R. (2016). A statistical study on the shape and position of the magnetotail neutral sheet. *Annales Geophysicae*, 34(2), 303–311. <https://doi.org/10.5194/angeo-34-303-2016>
- Xu, Z., Hartinger, M. D., Oliveira, D. M., Coyle, S., Clauer, C. R., Weimer, D., & Edwards, T. R. (2020). Interhemispheric asymmetries in the ground magnetic response to interplanetary shocks: The role of shock impact angle. *Space Weather*, 18(3), e2019SW002427. <https://doi.org/10.1029/2019SW002427>
- Zhang, G., & Burlaga, L. F. (1988). Magnetic clouds, geomagnetic disturbances, and cosmic ray decreases. *Journal of Geophysical Research*, 93(A4), 2511–2517. <https://doi.org/10.1029/JA093iA04p02511>
- Zhou, B., Cheng, B., Gou, X., Li, L., Zhang, Y., Wang, J., et al. (2019). First in-orbit results of the vector magnetic field measurement of the high precision magnetometer onboard the China seismo-electromagnetic satellite. *Earth Planets and Space*, 71(1), 119. <https://doi.org/10.1186/s40623-019-1098-3>